Femtosecond laser inscribed cladding waveguides in Nd:YAG ceramics: Fabrication, fluorescence imaging and laser performance

Hongliang Liu,[1] Yuechen Jia,[1] Javier Rodríguez Vázquez de Aldana,[2] Daniel Jaque,[3] and Feng Chen[1,*]

[1]*School of Physics, State Key Laboratory of Crystal Materials and Key Laboratory of Particle Physics and Particle Irradiation, Ministry of Education, Shandong University, Jinan 250100, China*
[2]*Laser Microprocessing Group, Universidad de Salamanca, Salamanca 37008, Spain*
[3] *Departamento de Física de Materiales, Facultad de Ciencias, Universidad Autónoma de Madrid, Madrid 28049, Spain*
[*]*drfchen@sdu.edu.cn*

Abstract: We report on the fabrication of depressed cladding waveguide lasers in Nd:YAG (neodymium doped yttrium aluminum garnet, Nd:$Y_3Al_5O_{12}$) ceramics microstructured by femtosecond laser pulses. Full control over the confined light spatial distribution is demonstrated by the fabrication of high contrast waveguides with hexagonal, circular and trapezoidal configurations. The confocal fluorescence measurements of the waveguides reveal that the original luminescence features of Nd^{3+} ions are well-preserved in the waveguide regions. Under optical pump at 808 nm, cladding waveguides showed continuous wave efficient laser oscillation. The maximum output power obtained at 1064.5 nm is ~181 mW with a slope efficiency as high as 44%, which suggests that the fabricated Nd:YAG ceramic waveguides are promising candidates for efficient integrated laser sources.

OCIS codes: (140.3390) Laser materials processing; (230.7380) Waveguides, channeled; (130.3120) Integrated optics devices.

References and links

1. E. J. Murphy, *Integrated Optical Circuits and Components* (Marcel Dekker, New York, 1999).
2. C. Grivas, "Optically pumped planar waveguide lasers, Part I: Fundamentals and fabrication techniques," Prog. Quantum Electron. **35**(6), 159–239 (2011).
3. K. M. Davis, K. Miura, N. Sugimoto, and K. Hirao, "Writing waveguides in glass with a femtosecond laser," Opt. Lett. **21**(21), 1729–1731 (1996).
4. R. R. Gattass and E. Mazur, "Femtosecond laser micromachining in transparent materials," Nat. Photonics **2**(4), 219–225 (2008).
5. M. Ams, G. D. Marshall, P. Dekker, J. Piper, and M. Withford, "Ultrafast laser written active devices," Laser Photon. Rev. **3**(6), 535–544 (2009).
6. A. Zoubir, C. Lopez, M. Richardson, and K. Richardson, "Femtosecond laser fabrication of tubular waveguides in poly(methyl methacrylate)," Opt. Lett. **29**(16), 1840–1842 (2004).
7. V. Apostolopoulos, L. Laversenne, T. Colomb, C. Depeursinge, R. P. Salathe, M. Pollnau, R. Osellame, G. Cerullo, and P. Laporta, "Femtosecond irradiation induced refractive-index changes and channel waveguiding in bulk Ti^{3+}:Sapphire," Appl. Phys. Lett. **85**(7), 1122–1124 (2004).
8. A. Rodenas and A. K. Kar, "High-contrast step-index waveguides in borate nonlinear laser crystals by 3D laser writing," Opt. Express **19**(18), 17820–17833 (2011).
9. T. Calmano, J. Siebenmorgen, F. Reichert, M. Fechner, A. G. Paschke, N. O. Hansen, K. Petermann, and G. Huber, "Crystalline Pr:$SrAl_{12}O_{19}$ waveguide laser in the visible spectral region," Opt. Lett. **36**(23), 4620–4622 (2011).
10. J. Burghoff, S. Nolte, and A. Tunnermann, "Origins of waveguiding in femtosecond laser structured $LiNbO_3$," Appl. Phys., A Mater. Sci. Process. **89**(1), 127–132 (2007).
11. Y. Tan, F. Chen, J. R. Vázquez de Aldana, G. A. Torchia, A. Benayas, and D. Jaque, "Continuous wave laser generation at 1064 nm in femtosecond laser inscribed Nd:YVO_4 channel waveguides," Appl. Phys. Lett. **97**(3), 031119 (2010).
12. Y. Tan, A. Rodenas, F. Chen, R. R. Thomson, A. K. Kar, D. Jaque, and Q. M. Lu, "70% slope efficiency from an ultrafast laser-written Nd:$GdVO_4$ channel waveguide laser," Opt. Express **18**(24), 24994–24999 (2010).

#170067 - $15.00 USD Received 8 Jun 2012; revised 25 Jul 2012; accepted 27 Jul 2012; published 31 Jul 2012

13. Y. Y. Ren, N. N. Dong, J. Macdonald, F. Chen, H. J. Zhang, and A. K. Kar, "Continuous wave channel waveguide lasers in Nd:$LuVO_4$ fabricated by direct femtosecond laser writing," Opt. Express **20**(3), 1969–1974 (2012).
14. T. Calmano, A. G. Paschke, J. Siebenmorgen, S. T. Fredrich-Thornton, H. Yagi, K. Petermann, and G. Huber, "Characterization of an Yb:YAG ceramic waveguide laser, fabricated by the direct femtosecond-laser writing technique," Appl. Phys. B **103**(1), 1–4 (2011).
15. T. Calmano, J. Siebenmorgen, O. Hellmig, K. Petermann, and G. Huber, "Nd:YAG waveguide laser with 1.3 W output power, fabricated by direct femtosecond laser writing," Appl. Phys. B **100**(1), 131–135 (2010).
16. J. Siebenmorgen, K. Petermann, G. Huber, K. Rademaker, S. Nolte, and A. Tünnermann, "Femtosecond laser written stress-induced Nd:$Y_3Al_5O_{12}$ (Nd:YAG) channel waveguide laser," Appl. Phys. B **97**(2), 251–255 (2009).
17. A. Rodenas, A. Benayas, J. R. Macdonald, J. Zhang, D. Y. Tang, D. Jaque, and A. K. Kar, "Direct laser writing of near-IR step-index buried channel waveguides in rare earth doped YAG," Opt. Lett. **36**(17), 3395–3397 (2011).
18. C. Zhang, N. N. Dong, J. Yang, F. Chen, J. R. Vázquez de Aldana, and Q. M. Lu, "Channel waveguide lasers in Nd:GGG crystals fabricated by femtosecond laser inscription," Opt. Express **19**(13), 12503–12508 (2011).
19. A. G. Okhrimchuk, A. V. Shestakov, I. Khrushchev, and J. Mitchell, "Depressed cladding, buried waveguide laser formed in a YAG:Nd3+ crystal by femtosecond laser writing," Opt. Lett. **30**(17), 2248–2250 (2005).
20. A. Okhrimchuk, V. Mezentsev, A. Shestakov, and I. Bennion, "Low loss depressed cladding waveguide inscribed in YAG:Nd single crystal by femtosecond laser pulses," Opt. Express **20**(4), 3832–3843 (2012).
21. D. G. Lancaster, S. Gross, H. Ebendorff-Heidepriem, K. Kuan, T. M. Monro, M. Ams, A. Fuerbach, and M. J. Withford, "Fifty percent internal slope efficiency femtosecond direct-written Tm^{3+}ZBLAN waveguide laser," Opt. Lett. **36**(9), 1587–1589 (2011).
22. N. Dong, F. Chen, and J. R. Vázquez de Aldana, "Efficient second harmonic generation by birefringent phase matching in femtosecond laser inscribed KTP cladding waveguides," Phys. Status Solidi **6**(7), 306–308 (2012).
23. Y. Jia, J. R. Vazquez de Aldana, C. Romero, Y. Ren, Q. Lu, and F. Chen, "Femtosecond-laser-inscribed BiB_3O_6 nonlinear cladding waveguide for second-harmonic generation," Appl. Phys. Express **5**(7), 072701 (2012).
24. Y. Liao, J. Xu, Y. Cheng, Z. Zhou, F. He, H. Sun, J. Song, X. Wang, Z. Xu, K. Sugioka, and K. Midorikawa, "Electro-optic integration of embedded electrodes and waveguides in $LiNbO_3$ using a femtosecond laser," Opt. Lett. **33**(19), 2281–2283 (2008).
25. S. J. Beecher, R. R. Thomson, D. T. Reid, N. D. Psaila, M. Ebrahim-Zadeh, and A. K. Kar, "Strain field manipulation in ultrafast laser inscribed BiB_3O_6 optical waveguides for nonlinear applications," Opt. Lett. **36**(23), 4548–4550 (2011).
26. R. Mary, S. J. Beecher, G. Brown, R. R. Thomson, D. Jaque, S. Ohara, and A. K. Kar, "Compact, highly efficient ytterbium doped bismuthate glass waveguide laser," Opt. Lett. **37**(10), 1691–1693 (2012).
27. A. Ikesue, Y. L. Aung, T. Taira, and G. L. Messing, "Progress in ceramic lasers," Annu. Rev. Mater. Res. **36**(1), 397–429 (2006).
28. F. Chen, Y. Tan, and D. Jaque, "Ion-implanted optical channel waveguides in neodymium-doped yttrium aluminum garnet transparent ceramics for integrated laser generation," Opt. Lett. **34**(1), 28–30 (2009).
29. Y. Tan and F. Chen, "Proton implanted optical channel waveguides in Nd:YAG laser ceramics," J. Phys. D **43**(7), 075105 (2010).
30. Y. Tan, C. Zhang, F. Chen, F. Q. Liu, D. Jaque, and Q. M. Lu, "Room-temperature continuous wave laser oscillations in Nd:YAG ceramic waveguides produced by carbon ion implantation," Appl. Phys. B **103**(4), 837–840 (2011).
31. G. A. Torchia, P. F. Meilán, A. Rodenas, D. Jaque, C. Mendez, and L. Roso, "Femtosecond laser written surface waveguides fabricated in Nd:YAG ceramics," Opt. Express **15**(20), 13266–13271 (2007).
32. G. A. Torchia, A. Rodenas, A. Benayas, E. Cantelar, L. Roso, and D. Jaque, "Highly efficient laser action in femtosecond-written Nd:yttrium aluminum garnet ceramic waveguides," Appl. Phys. Lett. **92**(11), 111103 (2008).
33. F. Chen, "Micro-and submicrometric waveguiding structures in optical crystals produced by ion beams for photonic applications," Laser Photon. Rev. DOI 10.1002/lpor.201100037.
34. I. Horcas, R. Fernández, J. M. Gómez-Rodríguez, J. Colchero, J. Gómez-Herrero, and A. M. Baro, "WSXM: a software for scanning probe microscopy and a tool for nanotechnology," Rev. Sci. Instrum. **78**(1), 013705 (2007).
35. J. Siebenmorgen, T. Calmano, K. Petermann, and G. Huber, "Highly efficient Yb:YAG channel waveguide laser written with a femtosecond-laser," Opt. Express **18**(15), 16035–16041 (2010).
36. A. Ródenas, G. A. Torchia, G. Lifante, E. Cantelar, J. Lamela, F. Jaque, L. Roso, and D. Jaque, "Refractive index change mechanisms in femtosecond laser written ceramic Nd:YAG waveguides: micro-spectroscopy experiments and beam propagation calculations," Appl. Phys. (Berl.) **95**(1), 85–96 (2009).
37. J. Lamela, A. Ródenas, D. Jaque, F. Jaque, G. A. Torchia, C. Mendez, and L. Roso, "Field optical and micro-luminescence investigations of femtosecond laser micro-structured Nd:YAG crystals," Opt. Express **15**(6), 3285–3290 (2007).

1. Introduction

As the basic elements in integrated photonics, optical waveguide structures can confine the light propagation in small volumes, achieving high optical intensities with respect to bulk materials, in which high-performance photonic devices could be constructed in small circuits

#170067 - $15.00 USD Received 8 Jun 2012; revised 25 Jul 2012; accepted 27 Jul 2012; published 31 Jul 2012

[1]. Benefiting from the compact geometry, waveguide lasers usually reach reduced lasing thresholds and comparable efficiencies in respect to bulk laser systems [2]. Femtosecond (fs) laser inscription has recently become a powerful and unique technique to fabricate waveguides in a wide range of optical materials [3–26], since Davis *et al.* reported their pioneer work in glasses [3]. Depending on the diverse parameters of the fs laser pulses and the material properties, the fs-laser micromachined waveguides can be with directly written structures (so-called Type I waveguide with single line writing), stress-induced waveguides (Type II with double line filaments), and depressed cladding waveguides. Compared with the wide application of Type I waveguides in numerous glasses and $LiNbO_3$ crystal [10], and Type II waveguides in some laser crystals (e.g., Nd:YVO_4 [11], Nd:$GdVO_4$ [12], Nd:$LuVO_4$ [13], rare-earth doped YAG crystals [14–17], Nd:GGG [18]) and $LiNbO_3$ [10], the cladding structures receive less attention from the scientific community. The cladding waveguides could be fabricated with arbitrarily designed cross sections by using direct fs-laser irradiation. Particularly, the scales of the cladding waveguide cross section could be designed to match the diameters of the multimode fibers; consequently, the fiber-waveguide-fiber integrated photonic chips may be constructed by using the depressed cladding structures. As of yet, such depressed cladding structures have been fabricated in laser materials, such as Nd:YAG single crystal [19, 20] and Tm:ZBLAN glass [21]. More recently, we have fabricated nonlinear depressed cladding waveguides in $KTiOPO_4$ and BiB_3O_6 crystals by using fs-laser writing, which shows enhanced optical conversion efficiency for green light second harmonic generation under birefringent phase-matching configuration with respect to the stress-induced $KTiOPO_4$ waveguide [22, 23]. In the cladding structures, the waveguide are located in the regions surrounded by the fs-laser induced tracks with negative refractive-index changes.

Supposed to be the next-generation high-efficiency gain media for solid state lasers, polycrystalline Nd:YAG ceramics have attracted broad attention owing to their outstanding fluorescent and laser properties [27]. Compared with the Nd:YAG single crystal, the ceramics can be obtained with larger dimensions and comparable laser performance. In addition, owing to the advantages of the fabrication technique, larger neodymium ion concentration could be achieved without degradation in the optical properties, at variance with their crystalline partners. With combination of such advantages of the Nd:YAG ceramics and waveguide platform, it is very intriguing to construct a compact, cost-effective laser source for various photonic applications. As of yet, the Nd:YAG ceramic waveguides have been produced by the ion implantation/irradiation [28–30] and the double-line fs-laser inscription [31], and waveguide lasers have been realized [32, 33].

In this work, we report on the fabrication of depressed cladding waveguides with three different geometries in Nd:YAG ceramics by using fs laser inscription. Confocal fluorescence images of the structures reveal the good preservation of the original fluorescence properties of Nd:YAG in the active volume. Finally, we also report on the continuous wave (cw) laser performance of the inscribed waveguides at 1.06 μm by using an end-pumping geometry.

2. Experimental

The optically polished Nd:YAG (doped by 2 at.% Nd^{3+} ions, obtained from Baikowski Ltd., Japan) ceramic wafer used in this work was with dimensions of 8 mm × 2 mm × 8 mm. The depressed cladding structures were produced by using an amplified Ti:sapphire laser system (Spitfire, Spectra Physics, generating linearly polarized 120 fs pulses at 800 nm, with 1 kHz repetition rate and 1 mJ maximum pulse energy) at the Universidad de Salamanca, Spain. The fs laser beam was focused by a microscope objective (Leica 40 × , numerical aperture N. A. = 0.65) and the pulse energy was set between 0.2 and 0.4 μJ with the help of a calibrated neutral density filter, a half-wave plate and a linear polarizer. The sample was placed in a motorized 3-axes stage and it was scanned at a constant velocity (700 μm/s), producing parallel damage filaments with separations of 3-4 μm at certain depths of the sample. Three structures with different configurations were fabricated.

The fluorescence images of the different fabricated structures were obtained in a home-made confocal microscope (See Fig. 1 for schematic plot of the experimental setup). The

#170067 - $15.00 USD Received 8 Jun 2012; revised 25 Jul 2012; accepted 27 Jul 2012; published 31 Jul 2012

optical excitation was provided by a 488 nm cw diode laser, which was focused into the sample by using a 100 × microscope objective with a N. A. of 0.85. The 488 nm spot size (radius) formed at sample's surface was estimated to be ~0.7 μm. The subsequent emission generated by Nd^{3+} ions was collected by the same microscope objective and after passing through different filters, lenses and pinholes was spectrally analyzed by a high resolution spectrometer. The sample was mounted onto to a three dimensional piezoelectric stage with an overall spatial resolution better than 10 nm. Both the spectrometer and the translation stage were simultaneously controlled in such a way that it was possible to scan the 488 nm excitation spot over the waveguide's cross section while acquiring the per-point emission spectrum. The acquired spectra were then spectrally analyzed and fitted by using the software LabSpec® so that it was possible to obtain fluorescence images of the waveguides in terms of the different fluorescence properties (namely spectral position, width and intensity of fluorescence lines). The fluorescence images were finally processed by using the software WSMP® [34].

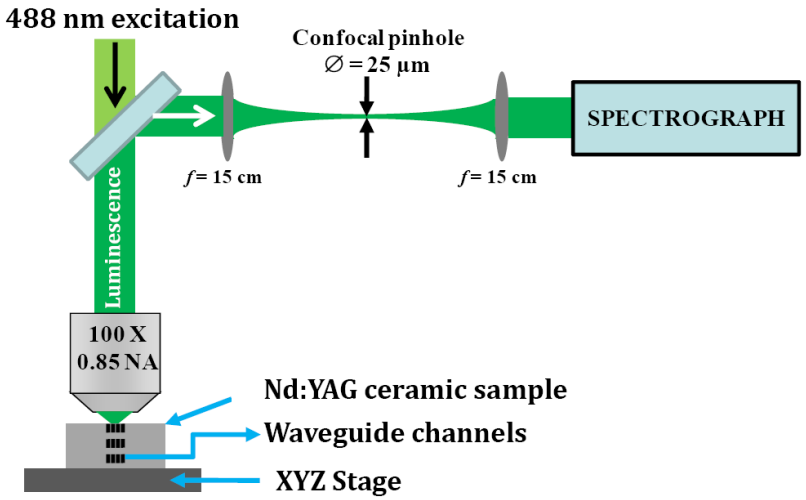

Fig. 1. Schematic of the experimental setup used for the micro-fluorescence investigation of the Nd:YAG ceramic cladding waveguides.

The waveguide laser experiments were performed under an end-pumped arrangement. A cw 808 nm linearly polarized pump beam from a Ti:sapphire laser (Coherent MBR 110), as the pump beam, was coupled into the waveguide by using a convex lens (with focal length of 25 mm). The output lasers from the waveguide's exit facet was collected by a 20 × microscope objective and imaged by an infrared CCD camera. Two dielectric mirrors (the input one was with reflectivity >99% at 1060-1065 nm and transmission of 98% at 800-810 nm, and the output one was with reflectivity >99% at 800-810 nm and transmission of ~60% at 1060-1065 nm) were adhered to the two end faces to construct a Fabry-Perot oscillating cavity. The output coupler of the waveguide laser system was then determined to be 60%. The length of the laser cavity was 8 mm. The generated laser radiation at IR wavelength was imaged by a CCD camera and characterized by a spectrometer and a powermeter.

#170067 - $15.00 USD Received 8 Jun 2012; revised 25 Jul 2012; accepted 27 Jul 2012; published 31 Jul 2012

2. Results and discussion

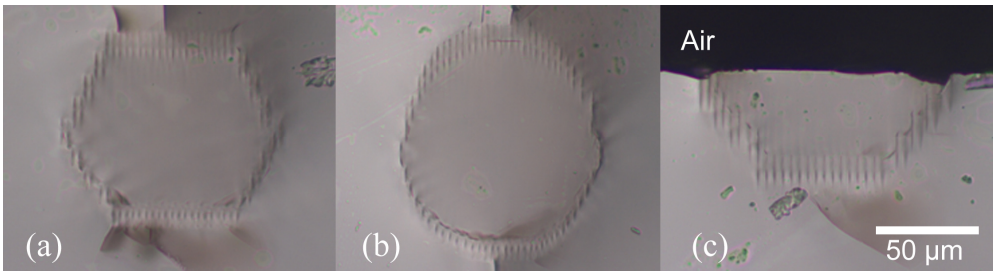

Fig. 2. Optical transmission microscope image of the depressed cladding (a) hexagonal, (b) circular and (c) trapezoidal waveguides in Nd:YAG ceramic. The scale bar for the three images is same.

Figures 2(a), 2(b) and 2(c) show the optical transmission microscope images of the depressed cladding waveguides as fabricated with hexagonal, circular and surface trapezoidal geometries, respectively. The hexagonal and circular waveguides were formed inside the sample at the depth of 70 μm beneath the surface.

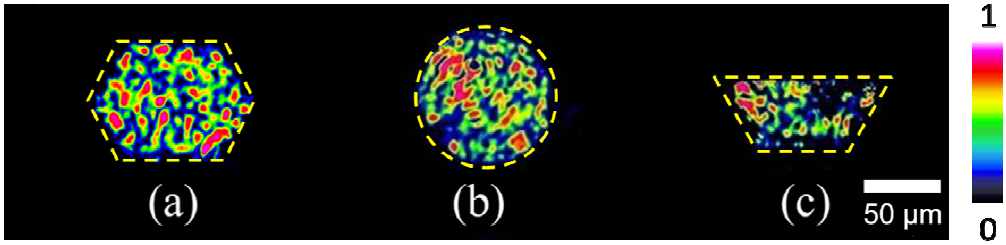

Fig. 3. The near field modal profiles of (a) hexagonal, (b) circular and (c) trapezoidal cladding waveguides in Nd:YAG ceramic at 632.8 nm. The dashed lines indicate the spatial location of the boundaries of the structures.

To investigate the guiding properties of the structures, we utilized an end-face coupling setup to observe the near field intensity distributions (at a wavelength of 632.8 nm). Figures 3(a), 3(b) and 3(c) depict the modal profiles of the hexagonal, circular and trapezoidal waveguides, respectively. As one can see, at 632.8 nm, all the three waveguides are multimode, and the boundaries of the near-field images are in good agreement with the respective geometries of the structures. We also found that the waveguides supported both TE and TM polarizations. By assumption of a refractive step index profile and from the experimentally obtained, the refractive index change taking place at filaments in respect to bulk can be estimated from [35]

$$\Delta n = \frac{\sin^2 \Theta_m}{2n}. \qquad (1)$$

where n is the refractive index of the bulk material, and Θ_m is the maximum incident angle at which the transmitted power is occurring without any change. According to the measured Θ_m we estimated the refractive index contrast $\Delta n \approx 2.2 \times 10^{-3}$ between the inscribed tracks and the waveguide regions. This value is in good agreement with the fs-laser induced index changes of the Nd:YAG single crystal cladding waveguides [20]. Nevertheless, this approach offers only a rough estimation of the refractive index changes in the filaments induced by the fs laser pulses. Further investigations are required on the physical mechanisms of the refractive index modifications to obtain more accurate values.

#170067 - $15.00 USD Received 8 Jun 2012; revised 25 Jul 2012; accepted 27 Jul 2012; published 31 Jul 2012

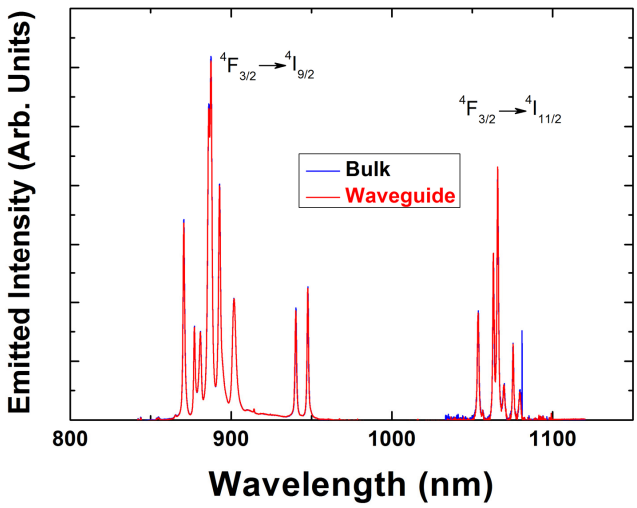

Fig. 4. Room-temperature fluorescence emission spectrum (μPL) related to the $^4F_{3/2} \rightarrow {}^4I_{9/2}$ and $^4F_{3/2} \rightarrow {}^4I_{11/2}$ transition of Nd^{3+} ions obtained from the femtosecond laser inscribed cladding waveguides in Nd:YAG ceramics (red solid line) and bulk of Nd:YAG sample (blue solid line).

Figure 4 depicts the confocal μPL emission spectra related to the $^4F_{3/2} \rightarrow {}^4I_{9/2}$ and $^4F_{3/2} \rightarrow {}^4I_{11/2}$ transitions of Nd^{3+} ions as obtained from a non-processed area (bulk) and from the center of the hexagonal structure (waveguide volume). Both emission spectra are virtually identical indicating that, basically, the fluorescence properties of Nd^{3+} ions at the waveguide's volume have been preserved during the ultrafast laser inscription procedure. This is an outstanding feature since it means that the fabricated structures could constitute the basis of low-threshold, high-gain integrated laser sources. Similar properties were found from the circular and trapezoidal cladding waveguides.

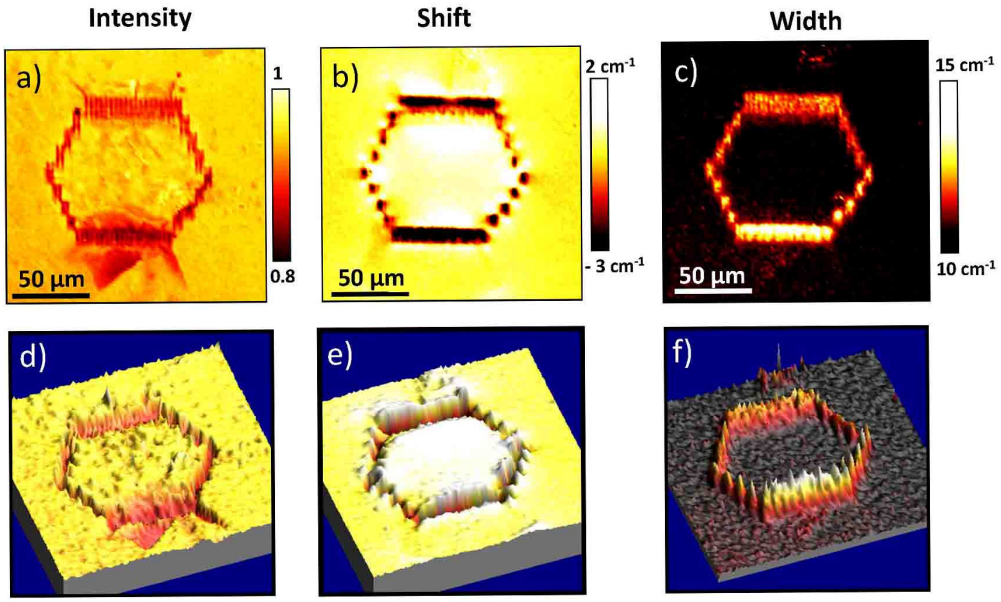

Fig. 5. Two-dimensional spatial distribution of the (a) emitted intensity, (b) energy shift and (c) FWHM of the Nd^{3+} emission lines obtained from the end face of the waveguide. (d), (e) and (f) correspond to the three-dimensional spatial distribution, respectively.

#170067 - $15.00 USD Received 8 Jun 2012; revised 25 Jul 2012; accepted 27 Jul 2012; published 31 Jul 2012

A detailed analysis of the emission spectra reveal that slight changes in both the spectral position and width of the different emission lines have been produced during ultrafast laser inscription. This is clear evidenced in the fluorescence images included in Fig. 5 that correspond to the cladding waveguide with the hexagonal geometry. Images correspond to the intensity, induced spectral shift and broadening of the Nd^{3+} fluorescence line at around 940 nm. This line is commonly used for fluorescence images of Nd:YAG devices because it is well isolated from other lines and also because it shows and hyper-sensitivity to small changes in the Nd^{3+} environments (such as strain, volume changes, disorders, and so on) [36]. From the first image it is clear that the fluorescence intensity is only reduced at the waveguide contour, where damage filaments are created. This is explained in terms of the high density of defects induced at these locations as a consequence of the localized optical breakdown. According to previous works [36] this localized damage causes a low-index barrier that confines light within the structure. As commented above, the intensity map also denotes a good preservation of fluorescence efficiency at the waveguide's volume. The fluorescence image obtained in terms of induced spectral shift (shown in the middle column in Fig. 5) also denotes a strong luminescence modification at the waveguide's contour. A strong luminescence shift towards lower energies (red-shift) has been produced at the damage contour. This is in accordance with the fluorescence images of Type-II waveguides in Nd:YAG [36] and it is attributed to a local compression of the Nd:YAG network as a consequence of the femtosecond laser induced optical breakdown caused in the Nd:YAG network. Note that at the waveguide's volume the fluorescence lines have been shifted towards larger energies (blue shift). We state that this blue-shift reflects a partial dilatation of the Nd:YAG network as a natural elastic response to the highly localized compression produced at the waveguide's contour. Finally, the fluorescence image obtained in terms of the spectral width denotes a large broadening of the fluorescence lines at the waveguide's contour. This, again, can be attributed to a local disordering of the Nd:YAG network as a consequence of the optical damage caused by the tightly focused laser pulses. This is, indeed, consistent with the fluorescence quenching observed at the waveguide's contour. Therefore, the fluorescence images included in Fig. 5 indicate that in our cladding waveguides the Nd:YAG network has been strongly modified only at the waveguide's contour, where the Nd:YAG network has simultaneously damaged, compressed and disordered. At the waveguide's volume, the Nd:YAG network has been only slightly modified, resulting in a partial dilatation that is not accompanied by any relevant disorder nor damage.

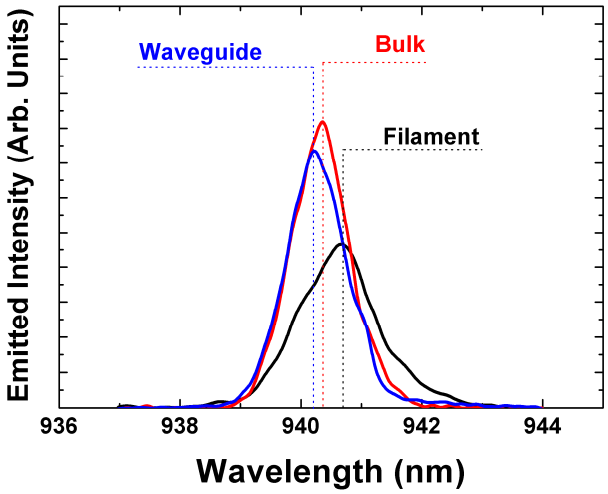

Fig. 6. Spectra of the Nd^{3+} emission lines at 940 nm for the three different positions (i.e., waveguide, damage filaments and bulk).

#170067 - $15.00 USD Received 8 Jun 2012; revised 25 Jul 2012; accepted 27 Jul 2012; published 31 Jul 2012

Details of the emission spectra related to 940 nm line of Nd^{3+} ions at the waveguide, damage filaments and bulk material are shown in the Fig. 6. As can be observed, the emission lines at waveguide area and bulk material have similar peak position and FWHM. Whilst, the peak shift and line broadening happened at the damage filaments are clearly observed. This detailed graph of 940 nm emission lines explained the emitted intensity, energy shift and FWHM of the Nd^{3+} emission lines (shown in Fig. 5) clearly.

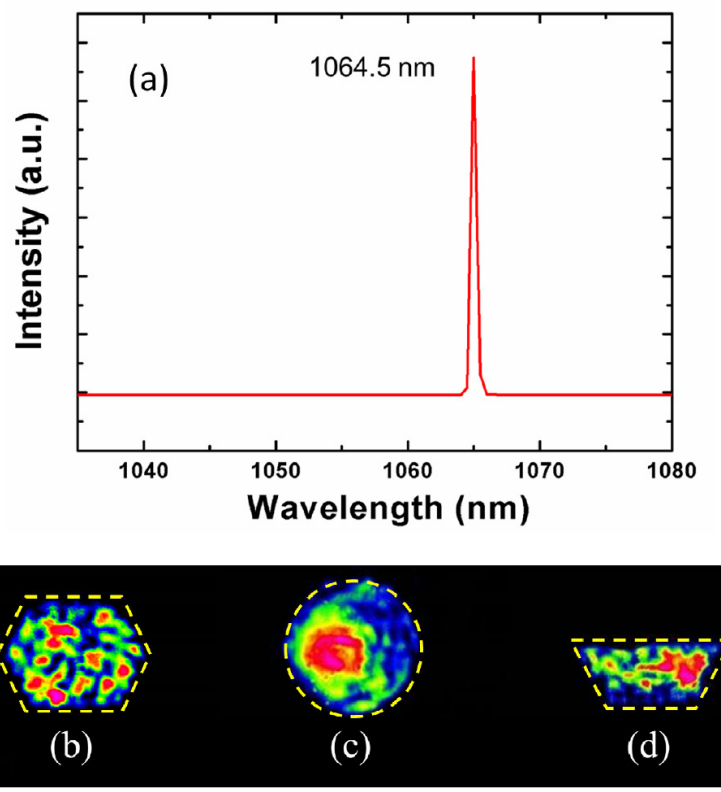

Fig. 7. (a) The cw laser emission spectrum from the Nd:YAG ceramic waveguide. The FWHM is ~0.6 nm. The waveguide laser modal distributions of (b) hexagonal, (c) circular and (d) trapezoidal waveguides at 1064.5 nm under 808 nm optical pump.

Once the structural and fluorescence properties of the fabricated structures are known, then their potential use of the fabricated structures as integrated laser sources has been evaluated by means of en-coupling experiments. Figure 7(a) shows the room temperature laser emission spectrum measured from the output end face of the Nd:YAG ceramic cladding waveguides. The sharp peak of the emission line is centered at 1064.5 nm, with a FWHM of ~0.6 nm. It is corresponding to the main transition line of the $^4F_{3/2} \rightarrow {}^4I_{11/2}$ transition of Nd^{3+} ions [37]. Figures 7(b), 7(c) and 7(d) depict the spatial modal profiles of the generated infrared waveguide lasers from the hexagonal, circular and trapezoidal structures, respectively. In addition, we also found that the light preserves the original polarization after propagation through the waveguide. The pump and lasing beams were with same polarizations. And the laser performance of the Nd:YAG ceramic waveguides was similar for TE and TM polarized light. Compared with the corresponding modal profiles at wavelength of 632.8 nm (Figs. 3(a), 3(b), and 3(c)), the infrared profiles of the waveguide lasers (Figs. 7(b), 7(c), and 7(d)) show obviously reduced mode numbers, which is reasonable according to the prediction of waveguide theory.

#170067 - $15.00 USD Received 8 Jun 2012; revised 25 Jul 2012; accepted 27 Jul 2012; published 31 Jul 2012

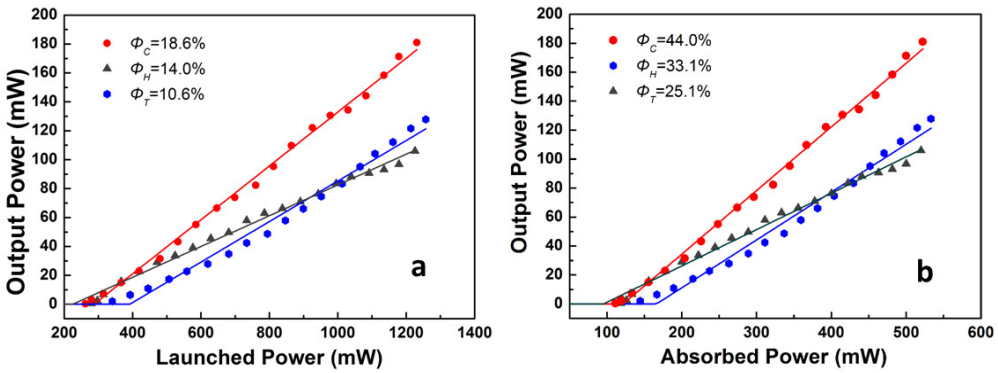

Fig. 8. The cw waveguide laser output power at 1064.5 nm as a function of the launched power (a) and the absorbed power (b) at 808 nm. The circular, hexagonal and triangular symbols stand for the data of the circular, hexagonal and trapezoid waveguides, respectively. The solid lines represent the linear fit of the experimental data.

Figures 8 (a) and 8(b) depict the dependence curves of the output cw waveguide laser power (at wavelength of ~1064.5 nm) on the launched power and the absorbed pump power (at wavelength of ~808 nm) from the circular, hexagonal, and trapezoidal structures, respectively. From the linear fit (solid lines) of the experiment data, the slope efficiency of the trapezoidal, hexagonal and circular waveguide laser are determined to be Φ_T = 10.6%, Φ_H = 14.0% and Φ_C = 18.6%, respectively, when the output power was depicted as a function of the launched one. By taking the coupling efficiency of the pump beam into the waveguides, one can obtain that the slope efficiency of the trapezoidal and hexagonal waveguide lasers are Φ_T = 25.1% and Φ_H = 33.1%, respectively, whilst it reaches Φ_C = 44.0% for the circular waveguide (Fig. 8(b)).The advantage for the trapezoidal waveguide laser is the lowest lasing threshold power ($P_{th,T}$ = 95.6 mW), whilst the other two waveguides exhibit higher thresholds ($P_{th,C}$ = 121.6 mW and $P_{th,H}$ = 160 mW, respectively). As for the maximum output power of the waveguide lasers at 1.06 μm, the trapezoidal, hexagonal and circular structures are $P_{out,T}$ = 106 mW, $P_{out,H}$ = 128 mW and $P_{out,C}$ = 181 mW, at absorbed pump 808-nm power of $P_{in,T}$ = 520 mW, $P_{in,H}$ = 530 mW, and $P_{in,C}$ = 522 mW, denoting optical conversion efficiency of 20.4%, 24.1% and 34.7%, respectively. The error of the experimental data (measured pump power values) is within 3%. The laser performances of the waveguides are determined by the coupling efficiency of the pump beam into the waveguide laser cavity and the propagation loss of the waveguides. The former is determined by the overlap of the pump beam field and the waveguide modal profiles. Under our pump system, the circular waveguide is with largest area of the cross section and circular shape of the modal field (fitting that of the pump beam), which means somehow the highest overlap of the pump beam and the waveguide modal profiles (effective area), resulting in highest efficiency; in addition, the circular waveguide is with lowest propagation loss (0.8 dB/cm); the high coupling efficiency and low propagation loss result in a high maximum output laser power among these three structures. The only drawback of this system is the lowest intensity of the pump beam, which increases the lasing threshold somehow. The hexagonal waveguide is with smaller area and the pump light coupled into the guiding core is more focused than that in the circular waveguide, however, the lasing threshold is higher in the hexagonal one, which may be due to the higher propagation loss (1.2 dB/cm). Moreover, the trapezoidal waveguide has the smallest effective area, which results in lowest lasing threshold, although the propagation loss of this structure is the highest (1.4 dB/cm). We also found that the ratio of the maximum output power and the optical conversion efficiency among the circular, hexagonal and trapezoid waveguides are ~1.75:1.2:1 and ~1.7:1.2:1, which are close to the ratio of the areas of the waveguides ~1.8:1.4:1. In principle, one could find a balance on the laser efficiencies and pump thresholds according to the practical requirement. The laser performance of the Nd:YAG ceramic waveguides is comparable to those reported in Nd:YAG single crystal cladding

#170067 - $15.00 USD Received 8 Jun 2012; revised 25 Jul 2012; accepted 27 Jul 2012; published 31 Jul 2012

waveguides [20]. Compared with the highly efficient stress-induced Nd:YAG waveguides, the advantage of the cladding waveguide systems is that the large cross sections of the cladding waveguides with circular cross sections are comparable to the multimode fibers of laser diodes (LD) for construction of fiber-waveguide platform, which makes them very promising for new LD pumped compact laser sources. This may be helpful to reduce the total costs of the waveguide laser system, and realize high output power waveguide lasers by taking the advantage of high-power, low cost LD pump lasers.

4. Summary

In summary, we have successfully fabricated depressed cladding Nd:YAG ceramic waveguides with different geometries by fs laser inscription. From the analysis of the confocal fluorescence images of the cladding structures we have identified the main physical mechanisms at the basis of waveguide formation. It has been concluded that the damage induced low refractive index barrier constituted by femtosecond laser induced optical breakdown is the main responsible of light confinement within the structures. Efficient laser operation at 1.06 μm of the fabricated waveguides has been demonstrated under 808 nm optical pump at 808 nm. The maximum output laser power is ~181 mW with a slope efficiency as high as ~44.0%. The excellent laser performance indicates potential applications of the fs-laser written Nd:YAG ceramic cladding waveguides as efficient integrated laser sources.

Acknowledgments

This work was supported by the National Natural Science Foundation of China (Nos. 10925524 and 11111130200), the Spanish Ministerio de Ciencia e Innovación (MICINN) through Consolider Program SAUUL CSD2007-00013 and Project FIS2009-09522. Support from the Centro de Láseres Pulsados (CLPU) was also acknowledged.

#170067 - $15.00 USD Received 8 Jun 2012; revised 25 Jul 2012; accepted 27 Jul 2012; published 31 Jul 2012